

## Intraurban Differences of Surface Energy Fluxes in a Central European City

B. OFFERLE

*Indiana University at Bloomington, Bloomington, Indiana, and Göteborg University, Göteborg, Sweden*

C. S. B. GRIMMOND

*Indiana University at Bloomington, Bloomington, Indiana*

K. FORTUNIAK AND W. PAWLAK

*University of Łódź, Łódź, Poland*

(Manuscript received 9 July 2004, in final form 13 June 2005)

### ABSTRACT

Surface properties, such as roughness and vegetation, which vary both within and between urban areas, play a dominant role in determining surface-atmosphere energy exchanges. The turbulent heat flux partitioning is examined within a single urban area through measurements at four locations in Łódź, Poland, during August 2002. The dominant surface cover (land use) at the sites was grass (airport), 1–3-story detached houses with trees (residential), large 2–4-story buildings (industrial), and 3–6-story buildings (downtown). However, vegetation, buildings, and other “impervious” surface coverage vary within some of these sites on the scale of the turbulent flux measurements. Vegetation and building cover for Łódź were determined from remotely sensed data and an existing database. A source-area model was then used to develop a lookup table to estimate surface cover fractions more accurately for individual measurements. Bowen ratios show an inverse relation with increasing vegetation cover both for a site and, more significant, between sites, as expected. Latent heat fluxes at the residential site were less dependent on short-term rainfall than at the grass site. Sensible heat fluxes were positively correlated with impervious surface cover and building intensity. These results are consistent with previous findings (focused mainly on differences between cities) and highlight the value of simple measures of land cover as predictors of spatial variations of urban climates both within and between urban areas.

### 1. Introduction

A significant number of surface energy balance studies of urban areas have been published in the last five years (Grimmond and Oke 2002; Christen and Vogt 2004; Grimmond et al. 2004; Offerle et al. 2005a). Most of these studies involve local-scale observations at only one or two sites within a city. As a consequence, inter-urban differences in the surface energy balance have been relatively well studied while intraurban variations and their significance have received much less attention, although the spatial variability would be expected to be similar. Grimmond and Oke (2002) showed that

local surface cover characteristics, such as fraction of vegetated and impervious surfaces or building morphology and density function as important controls on surface energy balance (SEB) fluxes in cities. Urban surface flux parameterizations that incorporate such relations are able to reproduce fluxes in good agreement with observations (Martilli et al. 2002; Masson et al. 2002; Grimmond and Oke 2002). Given that the spatial variability of surface cover can be as great within cities as between cities, it is reasonable to expect that significant differences in heat fluxes will occur across a city, for example, from a large park to the central business district (CBD). These differences are important because they can give rise to observable local climate effects such as the “park breeze” (Thorsson and Eliasson 2003). As computational resources have increased, the resolution of mesoscale models has improved so that not only are urban areas resolved but also the spatial

---

*Corresponding author address:* Brian Offerle, Urban Climate Group, Physical Geography, Göteborg University, Box 460, SE 405 30 Göteborg, Sweden.  
E-mail: bofferle@yahoo.com

variability within a city may be resolved when the urban area is large. This fact means that there is a need to know the spatial variability of surface cover and heat fluxes across the urban domain.

Schmid et al. (1991) found that the spatial variation of sensible heat flux  $Q_H$  within a single land use class, that is, suburban residential, was comparable to urban–rural differences. The variability in  $Q_H$  decreased with the increasing size of the estimated source area for the measurement, thus limiting the influence of small-scale surface inhomogeneities on the measured fluxes (Schmid et al. 1991). This result implies that the actual source-area characteristics determine flux partitioning and that using average characteristics independent of the flow characteristics in areas with sub-source-area heterogeneity may be imprecise. The use of generic descriptors of land use and land cover characteristics for meteorological modeling in urban areas will likely underestimate the spatial variability of surface–atmosphere exchange. Lemonsu et al. (2004) demonstrated that use of the default surface characterization for an area in Marseille, France, results in poorer performance of an urban land surface scheme than when the site-appropriate values are chosen.

Classifications of urban surfaces for meteorological modeling purposes are limited in the extent to which they can accurately represent the variation in surface characteristics and still remain generic. Examples of existing urban land use/land cover (LULC) classifications that considered meteorological characteristics as a rationale are Auer (1978), Ellefsen (1990), Grimmond and Souch (1994), and Theurer (1999). In general, the wide availability of remotely sensed data and existing spatial databases for urban areas make it possible to calculate surface characteristics for cities relatively simply without needing to rely on estimates from an LULC classification.

The primary objectives of this paper were to study the intraurban variation of the SEB through direct observation methods in a European city and to investigate the correlation between heat flux partitioning and physical properties of the surface that can be more easily and routinely measured. Field measurements were conducted during August–September 2002 in Łódź, Poland, around the urban area where long-term measurements of the SEB have been conducted since November of 2000 (Offerle et al. 2005a). Fluxes of net radiation  $Q^*$ , sensible heat, and latent heat  $Q_E$  were measured at each of the study sites. Surface properties fundamental in controlling the SEB were determined through ground sampling, remote sensing, and an existing surface database.

## 2. Methods

### a. Sites and measurements

Prior to the field campaign, aerial photographs (ca. 1994) were used to identify extensive, contiguous areas of homogeneous land cover representative of the major land use types: rural (RUR), suburban residential (RES), and industrial development (IND). Locations within the major land uses were selected based on the homogeneity of the surrounding land cover and the availability of a suitable measurement platform. Figure 1 shows the locations of the measurement sites and generalized land cover in Łódź. The long-term measurement site was located downtown in a dense urban CBD (Offerle et al. 2005a). The other sites, referred to collectively as “mobile,” used two sets of instrumentation that were relocated to different locations within 10 km of the long-term site. Therefore, only two mobile sites and the CBD site were operational at any one time.

For the CBD site, data from an Applied Technologies, Inc. (ATI; Boulder, Colorado), K-type sonic anemometer and a krypton hygrometer [Campbell Scientific, Inc. (CSI), Logan, Utah] mounted at 37 m above street level were used to calculate turbulent fluxes. A Kipp and Zonen CNR1 radiometer (Delft, Netherlands) was used to measure short- and longwave radiative fluxes. Data from a Rotronic Instrument Corporation (Huntington, New York) MP100H temperature and relative humidity probe at the same height were used to provide air temperature  $T_a$  and relative humidity (RH) for flux calculations. Further measurement details for this site are provided in Offerle et al. (2005a). Measurements at the mobile sites were conducted using a sonic anemometer (Model 81000, R. M. Young Company, Traverse City, Michigan), and either a krypton hygrometer (CSI) for water vapor flux measurements or an open-path infrared gas analyzer (LI-7500, Li-Cor, Inc., Lincoln, Nebraska) for both carbon dioxide ( $\text{CO}_2$ ) and water vapor. Net radiation  $Q^*$  was measured by Radiation and Energy Balance Systems, Inc. (REBS, Seattle, Washington),  $Q^*7.1$  net radiometers.

The instruments were mounted at heights exceeding 2 times the mean obstacle height; however, at IND the instruments were mounted 3 m above a 5 m  $\times$  5 m wide building, and at RES it was only possible to extend the boom for the instruments 1.5 m from the tower side, an open lattice structure of 2 m on a side. A listing of instrumentation and measurement heights for the sites is given in Table 1. Data from the sonic anemometers were processed into half-hourly statistics and fluxes,

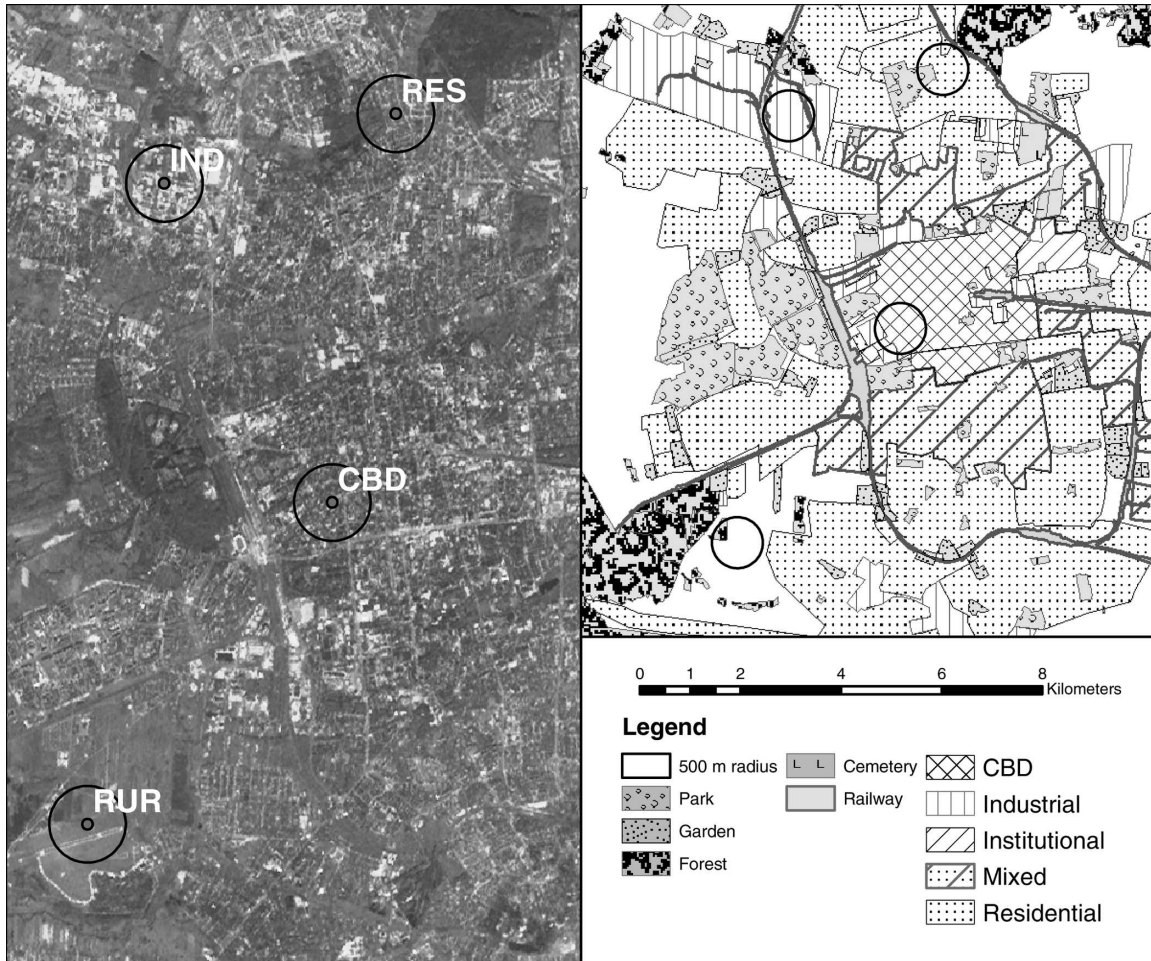


FIG. 1. (left) Locations of flux measurement sites overlaid on ASTER visible and near infrared (VNIR) (321) 17 Aug 2002. The circles show a radius of 500 m around the sites. (right) A simplified classification developed from aerial photographs and maps for land use and building types. Shaded areas are classified according to Łódź GIS. North is to the top of the map.

were block averaged, and were rotated to streamwise coordinates (Kaimal and Finnigan 1994). Corrections were applied for sonic virtual temperature (Schotanus et al. 1983), buoyancy effects on water vapor flux (Webb et al. 1980) and oxygen absorption for the krypton hygrometers (van Dijk et al. 2003). To ensure con-

sistency, data were excluded according to the criteria listed in Table 2.

The mast configuration at CBD made it possible to compare only one set of mobile instruments during the field campaign. The results show that these mobile instruments compared well to the long-term measure-

TABLE 1. Instruments used for energy balance flux measurements. Corrections from cross calibration of instruments are given where appropriate.

	CBD (long term)	Mobile 1		Mobile 2	
		RUR	IND	RES	CBD-M
Period (DOY 2002)	All days	228–235	235–245	228–239	241–245
$z_s$ (m)	37	2	23	41	35
Sonic anemometer	ATI K type	R. M. Young 81000		R. M. Young 81000	
Mean $\theta_v$ (offset, slope)		1.23, 0.99		1.23, 0.99	
H <sub>2</sub> O	Krypton	Krypton		LI-7500	
$Q^*$	CNR1	Q*7.1		Q*7.1	
Offset		-3.7		-4.2	
Multiplier ( $Q^* > 0$ , $Q^* < 0$ )		1.13, 1.17		1.16, 1.26	

TABLE 2. Criteria used for the acceptance of flux measurements. Subscripts refer to variable, i.e., velocity component ( $u$ ,  $v$ , and  $w$ ), sonic temperature ( $T$ ), or fast-response absolute humidity ( $\rho_v$ ).

Flux	Criteria
Momentum	No. of obs ( $N_{u,v,w}$ ) > 50% of possible No. of spikes detected ( $NS_{u,v,w}$ ) < 0.5% Vertical rotation angle ( $\varphi$ ) < 60° Variance ( $\sigma^2$ ): $\sigma_u^2 < 2.25$ , $\sigma_v^2 < 10$ , $\sigma_w^2 < 5$ , $0.01 < u_* < 2$ $0.1 < \text{wind speed} < 10$ *Rain, hourly = 0.0 mm, surface wetness (SW) > 10 k $\Omega$ , $\Delta \ln(\text{SW}) < -2$
Sensible heat	$N_T > 50\%$ , $NS_T < 0.5\%$ , $\sigma_T^2 < 2.25$ , $-100 < Q_H < 500$ , $ T - T_d  < 5^{**}$
Latent heat	$N_{\rho_v} > 50\%$ , $NS_{\rho_v} < 0.1\%$ , $\sigma_{\rho_v}^2 < 5$ , $-100 < Q_E < 500$ , $ \rho_v - \rho_v(\text{RH})  < 15$

\* From CBD location.

\*\* Only for CBD.

ment setup (Fig. 2). The net radiometers were compared later. Corrections for the mobile instruments were determined by ordinary least squares regression with separate coefficients for daytime ( $Q^* > 0$ ) and nighttime values (Kaminsky and Dubayah 1997; Brotzge and Duchon 2000) after first applying the manufacturer's correction for wind speed. The applied corrections for the instruments are given in Table 1. Sonic temperatures  $\theta_v$  were also corrected for measurement height relative to CBD. Because there is little topographic variation, this adjustment is small.

### b. Surface characteristics

Given the range of LULC schemes that are used in the literature to characterize sites and their use for meteorological modeling purposes, the class that would best characterize each site for a number of schemes is included in Table 3. However, surface characteristics here were determined from existing data sources and some additional ground sampling. Building height information was added to a vector geographic information system (GIS) of building footprints based on sampling carried out during the field campaign. About 75% of the sampled buildings were within 1 story of the estimated height, with a mean difference of 0.3 stories. The largest errors occur for tall buildings (relative to surrounding buildings); thus the height values underestimate the variance in building height. An Advanced Spaceborne Thermal Emission and Reflection Radiometer (ASTER) image acquired during the field campaign was used to determine the broadband albedo (Liang 2000) for all sites. Based on the results near CBD, where albedo was directly measured (0.08 in situ vs 0.10 ASTER), the estimate of albedo appears to be slightly

biased. Emissivity was determined directly from the ASTER level-II emissivity product (Abrams et al. 2002) averaged over the five thermal bands. Vegetation cover was determined based on the linear relation between the ASTER-calculated normalized difference vegetation index [NDVI;  $\text{NDVI} = (\text{band } 3 - \text{band } 2) / (\text{band } 3 + \text{band } 2)$ ] and vegetative surface fractions identified from the aerial photographs.

The roughness length for momentum was computed using anemometric and morphometric methods because modelers will have access only to this latter value or one based on a generic classification. The anemometric roughness length was computed by solving the stability-corrected (Panofsky and Dutton 1984) logarithmic law for  $z_{0M}$  based on an assumed zero-plane displacement height  $z_d$ . Data were restricted to local Monin–Obukhov stability parameter [ $\zeta = (z_s - z_d)/L$ , where  $z_s$  is the measurement height and  $L$  is the Obukhov length], between 0 and  $-0.1$ , and  $z_d$  was taken from the morphometric estimate. The Raupach (1994) morphometric method [selected based on Grimmond and Oke (1999a)] was determined from the average of cell values within 500 m of the tower locations without the inclusion of vegetation effects. These effects are important where trees are higher than the buildings and represent a large fraction of the surface cover such as for IND and RES and the  $z_d$  estimate would therefore be biased to be too low. Thus, as would be expected, the morphometric estimates differ most, by a factor of 2 or more, from the anemometric values in the cases of IND and RES (Table 3). The values for the CBD site correspond closely, being different by less than 10%.

Canyon aspect ratio  $H/W$  is most readily calculated for cases in which there is a bilateral symmetry about the street's long axis (Oke 1987). This condition is approximately true for the central core of the city but not for other areas with scattered buildings and is difficult to reconcile with street vegetation. The Table 3 values were estimated from road widths and building heights. The CBD value is approximately equal to that calculated from the road sky-view factor  $\psi$ . The average  $\psi$  from 40 digital fish-eye photos (Grimmond et al. 2001) for roads (not including intersections) in the CBD area was 0.54. Inverting the theoretical  $\psi$  equation for a symmetric infinite canyon (Oke 1987) gives an  $H/W$  of 0.78. The average  $\psi$  over all of the fish-eye photos taken in the CBD area was 0.62, giving an  $H/W$  of 0.63.

### c. Flux source-area estimation

It is a reasonable first approximation that the characteristics at each site be estimated using a simple area-

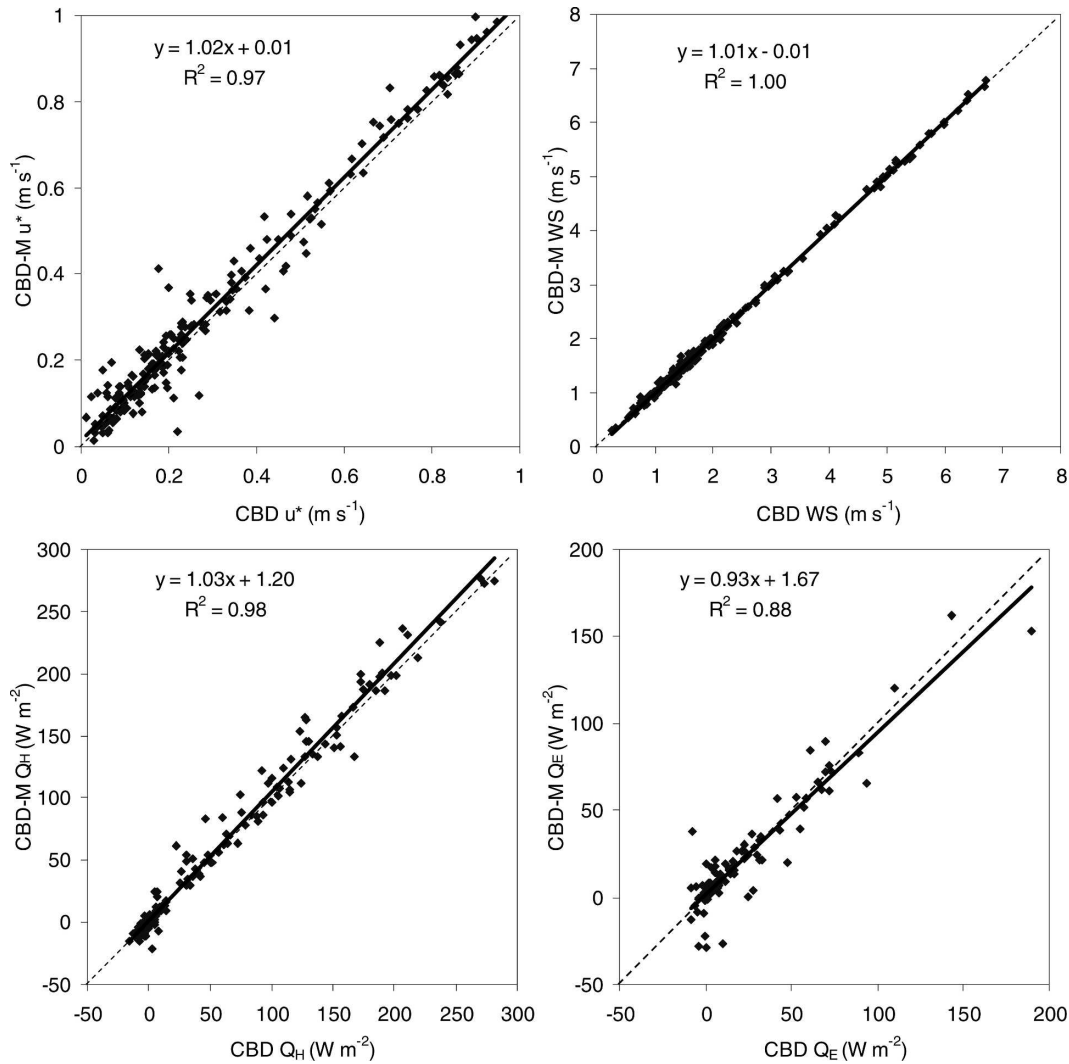


FIG. 2. Comparison of flux measurement systems at CBD. The mobile system, CBD-M, is mounted  $\sim 2$  m lower and nearer to the mast than the CBD system. The dashed and solid lines represent the 1:1 and best-fit linear regression, respectively. The line estimate and coefficient of determination ( $R^2$ ) are shown in each plot.

average approach, but the true surface characteristics will vary with each measurement because of changes in turbulence characteristics and stability. Over natural surfaces where ecosystem-scale representation is often an objective, Schmid and Lloyd (1999) demonstrated that smaller-scale surface inhomogeneities can result in a “sensor location bias,” meaning that the sensor does not measure the “true” ecosystem flux resulting from differences in the average surface characteristics between the observed source area and the average value of the ecosystem of interest. Therefore, a representative urban flux within many cities is difficult to obtain because of both the spatial heterogeneity and the lack of adequate extent of any particular agglomeration of constant surface characteristics. It is imperative that the

source areas be estimated to determine the surface characteristics of the actual measurements.

To determine the approximate source areas for the fluxes, the analytical flux source-area model (FSAM) of Schmid (1994) was used. Although it is recognized that this applies only to homogeneous surface layers, running a three-dimensional model was not considered because of the more comprehensive input required in terms of surface structure and turbulence parameterization within urban canyons. For all sites, a lookup table was created in three parameters: the Monin–Obukhov stability parameter  $\zeta$ , normalized transverse velocity standard deviation ( $\sigma_v/u_*$ , where  $u_*$  is friction velocity), and wind direction. The parameter set was as follows:  $\zeta = \{-0.5, -0.1, -0.05, 0, 0.05\}$ ,  $\sigma_v/u_* = \{1.5,$

TABLE 3. Characteristics of the measurement locations. Urban LULC classes are defined in the respective references.

Site ID	CBD	IND	RES	RUR
Land use	Commercial, institutional, residential	Industrial, commercial, power generation, residential	Residential	Airport
Land cover description	Dense urban attached structures	Low, long, narrow buildings	Single-family detached houses, some institutional and block houses	Open grass, perimeter trees, and some detached buildings
Roof	Flat to slightly pitched, tarred	Flat to slightly pitched, tarred, metal	Pitched, asphalt shingles, metal, or tiles	
Stories	3–6	2–4	1–3	
Walls	Concrete, brick	Concrete, brick	Wood, concrete, brick	
Vegetation	Deciduous street trees < building height	Deciduous street trees $\geq$ building height	Short grass, mixed deciduous, evergreen trees $\geq$ building height	Short grass (<0.1 m), tall grass, mixed herbaceous (0.1–0.3 m)
Other	Asphalt streets, pavements	Asphalt streets, pavements	Brick or asphalt streets, pavements	Sandy soil
Urban LULC class				
Auer (1978)	C1?	I2	R2	A1
Ellefsen (1990)	A2	Do4	Dc3–Do3	—
Grimmond and Souch (1994)	CB?	I	A	VGR
Theurer (1999)	CC–BEB	IA	SFH	GA
Ground elev (m)	204	204	210	182
Building height <sup>a</sup> $z_H$ (m)	10.2	8.5	7.7	0
Canyon aspect ratio $H/W$	0.75	0.4	0.3	0
Plan area index $\lambda_p$	0.3	0.2	0.1	0
Displacement height <sup>a,b</sup> $z_d$	7.4	3.6	1.8	0.38
Morphometric roughness length <sup>a,b</sup> $z_{0M}$	1.7	0.62	0.32	0.02
Anemometric roughness length $z_{0M}$	1.7 <sup>c</sup> /1.7 (mobile)	1.3	1.2	0.01
Albedo <sup>d</sup> $\alpha$	0.10 (0.08 <sup>c</sup> )	0.14	0.15	0.18
Emissivity <sup>d</sup> $\epsilon$	0.93	0.92	0.94	0.99

<sup>a</sup> Mean of values from within 500 m of measurement location from building dimensions only.

<sup>b</sup> Raupach (1994).

<sup>c</sup> Observation from long-term measurement location.

<sup>d</sup> ASTER derived.

2.5, 5.0}, and wind direction in 15° increments. This set resulted in a lookup table with 360 source areas for each site. Because unstable source areas are smaller, which may result in more variance among measurements, more categories were specified for these cases. The other site-specific parameters,  $(z_s - z_d)/z_{0M}$  and  $z_{0M}$ , were determined from the aerodynamic  $z_{0M}$  and morphometric  $z_d$ . The matrix of source-area weights (90%) was computed on a 1-m grid (cell size) for the RUR site and on a 10-m grid for the other sites. The fractions of vegetation, buildings, and impervious surfaces (other by residual) were determined. The source-area matrix was truncated for regions outside of the grid domain (500 × 500). The average results are given in Table 4 for unstable conditions, which are the times of greatest turbulent exchanges of heat.

At CBD the fraction of vegetation ranges from 0.14 to 0.4 with a mean of 0.27 ( $\zeta = -0.1$ ) (Offerle et al. 2005a). During this field campaign, for unstable conditions (Table 4) the vegetation fraction averaged 0.24 and building coverage, with a slightly smaller range, averaged 0.35. The residential site, originally a suburban development (Klysik 1996), has more vegetation and a lower housing density than the more recent residential developments that make up more of the city. The source area for this site included a large open field, about 250 m to the east, with a small channelized stream. In this area, tall grasses were the primary vegetation, although in the greater source area, trees, mostly deciduous and taller than building height, and well-irrigated lawns were dominant. At RES under unstable conditions, the mean vegetated surface fraction

TABLE 4. Spatial mean (standard deviation) of source-area surface characteristics (plan-area fraction) during measurement period for turbulent fluxes (unstable) using FSAM filter and net radiative fluxes using circular filter. Buildings (BLD) footprints were taken from a 10-m grid, and vegetation fraction (VEG) is from a 15-m grid. Impervious (IMP) surface cover other than buildings was determined as the residual.

Site	Unstable 90%			Radiometer 90%		
	BLD	VEG	IMP	BLD	VEG	IMP
CBD	0.35 (0.09)	0.24 (0.11)	0.41 (0.04)	0.34	0.34	0.32
IND	0.17 (0.02)	0.39 (0.14)	0.44 (0.12)	0.12	0.24	0.63
RES	0.10 (0.03)	0.78 (0.07)	0.13 (0.05)	0.15	0.74	0.11
RUR	0.00 (0.00)	1.00 (0.00)	0.00 (0.00)	0.00	1.00	0.00

was 0.78, with only 0.10 in buildings. The industrial site had a surprising amount of canopy-level vegetation (0.39, unstable), with most streets lined with trees as well as tree or grass cover over some abandoned or undeveloped areas. In terms of vegetated fraction IND fell between CBD and RES, with approximately the same impervious surface fraction as that of CBD.

Consideration must also be given to the source area of the net radiation measurement because any incongruities between surfaces in the field of view of the radiometer and the source area of the flux measurement could lead to an imbalance in the observed energy balance. For these sites, source-area characteristics for the net radiative fluxes (Schmid 1994) can differ from the unstable source areas by as much as 0.2 (Table 4), with the greatest differences occurring at IND.

### 3. Results and discussion

Synoptic conditions were consistent during most of the observation period, dominated by high pressure situated over the Baltic. Days were predominately clear and dry, with nighttime cloudiness being more variable. Stable conditions at CBD, though unusual over the longer term, occur on about one-half of the nights of this field campaign.

Wind speed did not vary significantly over the urban sites during the daytime, although on occasion higher values were recorded at RES. Even the RUR wind speed at 2-m height was within  $1 \text{ m s}^{-1}$  of CBD. At night RUR wind speeds were much lower, as would be expected, and RES was noticeably higher (not shown). Air temperature measured close to the surface is strongly impacted by local characteristics. The RUR site has the greatest diurnal range in  $\theta_v$  and is substantially cooler than CBD at night (Fig. 3). This can be seen as primarily a local effect resulting from the strong coupling with surface temperatures at this height. Tem-

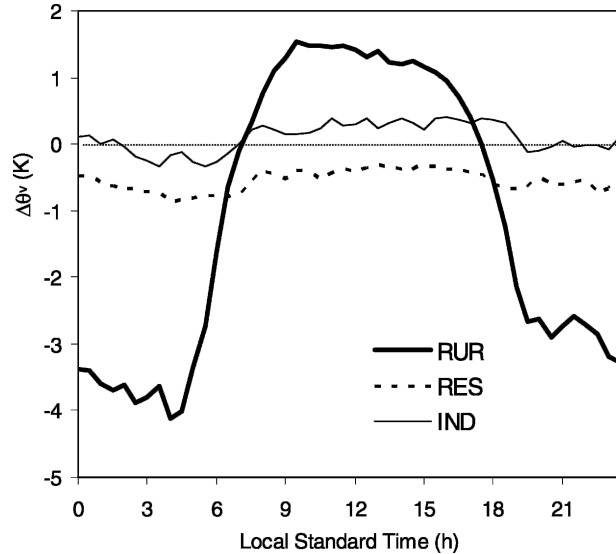


FIG. 3. Diurnal differences in sonic temperature  $\theta_v$  from CBD site.

peratures at RUR are slightly warmer by day and around  $3^{\circ}\text{--}4^{\circ}\text{C}$  lower at night, consistent with previous estimates of urban–rural temperature differences (Klysiak and Fortuniak 1999). The maximum RUR–CBD difference of approximately  $-8^{\circ}\text{C}$  occurs on the night of yearday (DOY) 234–235 when conditions were clear and calm (wind speed  $< 0.5 \text{ m s}^{-1}$  at CBD) as is typical for the nocturnal urban heat island (UHI). Temperatures for the other sites are more similar (Fig. 3), and they again vary as might be expected, with RES being slightly cooler than CBD, both day and night, and IND being slightly warmer by day. Because the heights of both CBD and RES are very similar, their difference may come closer to approximating a surface layer UHI effect, in this case around  $0.5^{\circ}\text{C}$ .

The most notable differences in diurnal patterns of net radiation also occur between RUR and the other sites. Figure 4 shows the diurnal differences in  $Q^*$  with reference to CBD. The mean midday difference between CBD and RUR can mostly be attributed to the difference in outgoing solar radiation (i.e., because of albedo). Measured solar radiation at CBD was over  $700 \text{ W m}^{-2}$  at midday, meaning  $56 \text{ W m}^{-2}$  more outgoing shortwave radiation at RUR, which is approximately equal to the midday difference in  $Q^*$  between the sites. This condition also requires approximately equivalent net longwave radiation at midday. Net radiation at RES and net radiation at CBD are similar in the daytime despite their different albedos, and thus the difference in outgoing longwave radiation between the two sites must balance the difference in net shortwave radiation (in this case about  $35 \text{ W m}^{-2}$ ). At IND the nighttime

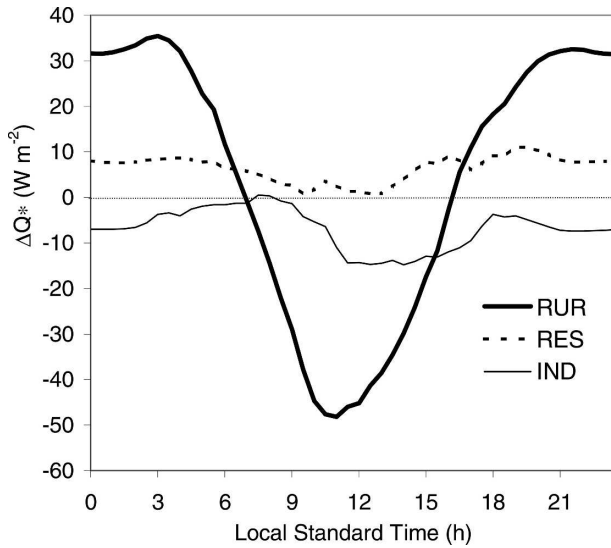


FIG. 4. Diurnal differences in net radiation from CBD.

difference suggests slightly higher outgoing longwave radiation. That net radiation should be spatially conservative across an urban area can be expected because differences in albedo are offset by differences in outgoing longwave radiation. Over the total course of a day, the differences in  $Q^*$  are small except at IND. The RES and RUR sites differ by 5% or less from CBD (Table 5). At the IND site, with a much higher impervious fraction in the radiometer source area,  $Q^*$  was 10% lower than at CBD. Christen and Vogt (2004) found similar small differences in a mix of urban and rural surface covers and a larger reduction in  $Q^*$  ( $-50\%$ ) over a concrete surface.

Thus, aside from the rural site, differences in the primary energetic forcing for the turbulent fluxes are small ( $Q^*$  and wind speed), and similar patterns between the

sites can be expected as Fig. 5 shows. The major differences between the sites concern the magnitude, timing, and partitioning of the turbulent fluxes, which are controlled to a large extent by surface characteristics, namely, the amount of active transpiring or evaporating surface and the thermal properties. At the more heavily built sites, CBD and IND,  $Q_H$  and  $Q_E$  increase nearly simultaneously, whereas at the primarily vegetated sites  $Q_H$  lags  $Q_E$ , with the greatest lag over the grass surface (Fig. 5). During the daytime  $Q_H$  is greater than  $Q_E$ . Of interest is that  $Q_E$  at the denser urban sites is generally greater at night than over RUR and RES. This situation could be a result of the nocturnal boundary layer air over the vegetated areas being more saturated and thus restricting latent heat transfer. In addition, the total heat storage over the daytime is greater in these areas, providing warmer surface temperatures and additional energy for evaporation because  $Q_H + Q_E$  is more frequently positive at night.

About 35 mm of rain fell during 8 days preceding the field campaign, including DOY 228, but during the study period measurable rainfall occurred only at the end, on DOY 241 and following days. Volumetric soil moisture (averaged to 150-mm depth) measured at CBD decreased over the entire period, from 20% to 12%. At RUR gravimetric samples from the upper 50 mm of soil decreased from 11.8% to 5.3% over the first 7 days. At the beginning of the measurement period (DOY 229 of 2002),  $Q_E$  at RUR initially was more than 2 times the magnitude of  $Q_H$ , but it dropped off to a daytime ratio close to 1 after 2 days. CBD and RES were less influenced by this earlier rainfall because trees make up a greater percentage of the nonimpervious surface, and much of the rainfall is channeled out of the system; however, the effects of the earlier rainfall were still apparent. During the dry period (DOY 232–

TABLE 5. Net radiation and flux partitioning ( $W m^{-2}$ ) over all observations and daytime. Here,  $Q^*$  CBD is the net radiation measured at CBD for the same observations periods as the mobile-site  $Q^*$  (see Table 1). Values given in parentheses for  $\Delta Q_S/Q^*$  daytime show results after daytime turbulent fluxes are adjusted so that storage is zero over the period.

Site	$Q^*$	$Q^*$ CBD	$Q_H$	$Q_E$	$\Delta Q_S$	$Q_H/Q^*$	$\beta^*$	$\Delta Q_S/Q^*$ <sup>a</sup>
				All				
CBD	99.6	99.6	55.8	38.8	5.0	0.56	1.45	0.05
IND	82.9	91.8	39.3	31.6	12.0	0.47	1.25	0.16
RES	107.7	102.4	36.6	58.5	12.6	0.34	0.64	0.13
RUR	133.2	135.6	27.6	89.4	16.3	0.21	0.29	0.10
				Day ( $Q^* > 0$ )				
CBD	292.1	292.1	127.5	68.4	96.1	0.44	1.83	0.32 (0.29)
IND	264.0	271.4	94.5	56.6	113.0	0.36	1.61	0.41 (0.31)
RES	304.9	299.1	90.9	112.5	101.5	0.30	0.80	0.32 (0.23)
RUR	290.2	314.0	64.7	156.8	68.6	0.22	0.41	0.24 (0.16)

<sup>a</sup> Results calculated from diurnally averaged values.

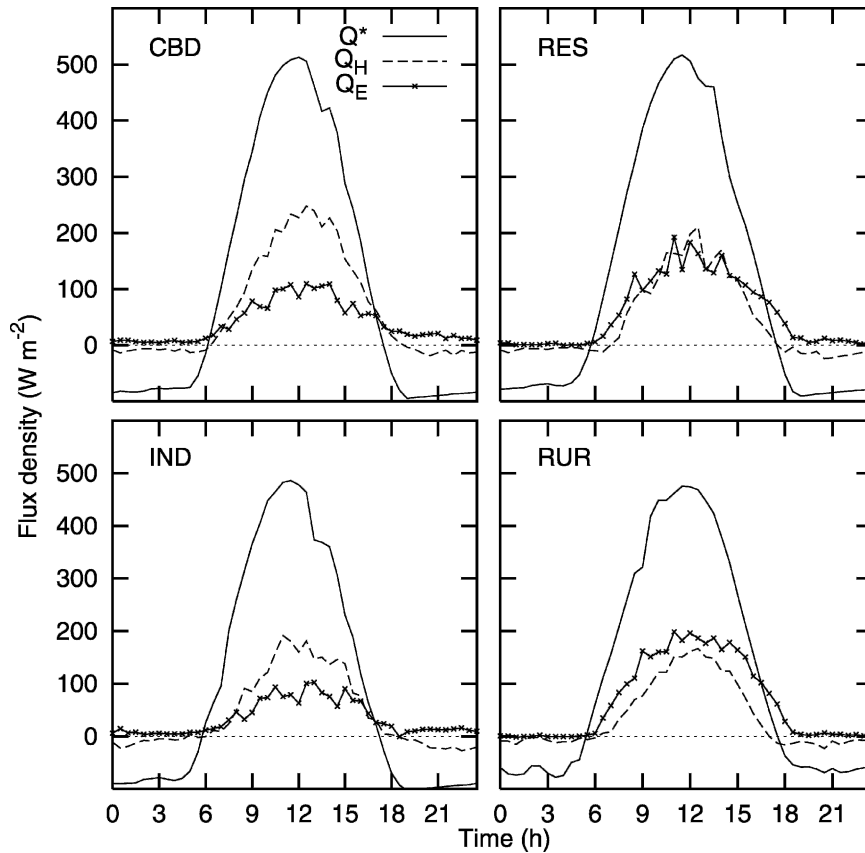


FIG. 5. Diurnal fluxes over the dry period of the campaign.

240) the influence of earlier rainfall was minimized, and the Bowen ratio ( $\beta = Q_H/Q_E$ ) varied inversely with the fraction of vegetated surface (Fig. 6). Figure 6 indicates that  $\beta$  shows a relation with the fraction of vegetation

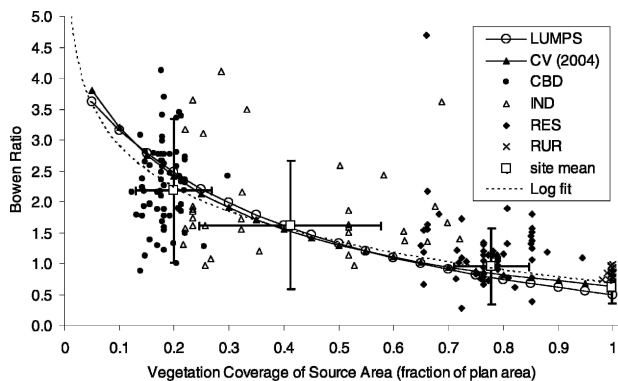


FIG. 6. Relation between source-area fraction of vegetation and observed Bowen ratio for dry period of campaign (DOY 232–240 of 2002) for daytime ( $Q^* > 0 \text{ W m}^{-2}$ ) and positive turbulent fluxes. The solid lines represent the LUMPS prediction (Grimmond and Oke 2002), and Christen and Vogt (2004) described in the text;  $X$  and  $Y$  error bars are  $\pm 1$  std dev. Site sample points are shown for 1000–1400 LST.

both between sites and within sites, although there is much scatter. Likewise, the ratio of turbulent sensible heat flux to available energy is positively correlated with total impervious surface (Fig. 7). This relation is important because it suggests that the fraction of the vegetated area can be used effectively as a method to partition the convective energy fluxes in land surface

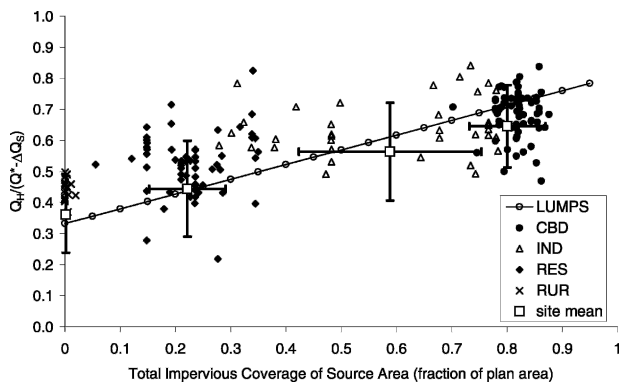


FIG. 7. Similar to Fig. 6, but relating total impervious surface to the sensible heat available energy ratio  $[Q_H/(Q^* - \Delta Q_S)]$ , where  $\Delta Q_S$  is the measured energy balance residual.

schemes in urban areas. Because the Bowen ratio is used in a number of schemes as a characteristic of a site/grid (Ross and Oke 1988) this approach provides a way of assigning a value a priori.

The Priestley and Taylor (1972, hereinafter PT) formulation for potential evaporation gives a latent heat flux of

$$Q_E = \frac{\alpha_{PT}}{1 + \frac{\gamma}{s}} (Q^* - \Delta Q_S), \quad (1)$$

where  $\alpha_{PT}$  is an empirically determined coefficient (approximately 1.26 for saturated land surfaces and open water),  $\gamma$  is the psychrometric constant, and  $s$  is the slope of the saturation vapor pressure curve for a given temperature. Sensible heat flux is then determined by  $Q^* - \Delta Q_S - Q_E$ . If one assumes an air temperature of 20°C and scales total evaporation by fraction of vegetation, the curve defined by (1) would result in a  $\beta$  of approximately 5 at 20% vegetated surface fraction. As  $\alpha$  is reduced to more realistic values, the predicted  $\beta$  increases, as expected, for a given vegetation fraction. A similar assumption occurs when a tile scheme is used in a grid of a mesoscale model (e.g., Masson 2000; Best 2005). The responses from the tiles are weighted by their areal fractions in the grid cell (see Fig. 2 of Best 2005) and do not interact at the subgrid scale. An alternative approach is to consider the surface as an integrated whole (see Fig. 2 of Grimmond and Oke 2002) that has separate fractions but for which the response is treated as a whole in the analysis. The de Bruin and Holtslag (1982) modification of the PT combination equation for actual evaporation using the coefficients specified in Grimmond and Oke (2002) [local-scale urban meteorological parameterization scheme (LUMPS)] is plotted in Fig. 6. In this case the surface is treated as the integrated whole. The LUMPS estimate, which was developed and evaluated over a wide range of urban observations (Grimmond and Oke 2002), shows good agreement with the values here (Fig. 6). The relation reported by Christen and Vogt (2004) for Basel, Switzerland, is very similar to the LUMPS estimate, although allowing for better agreement at the rural end because this is fixed by  $\beta_{RUR}$ . The site means suggest slightly lower Bowen ratios for the more impervious sites but well within one standard deviation of the mean.

If heat storage flux is assumed to be zero, the PT relation can be estimated for  $Q_H/Q^*$  (Fig. 7). To compare measured values where heat storage is nonzero, the sample data were referenced to available energy calculated as  $Q^* - \Delta Q_S$ , where  $\Delta Q_S$  is the residual

estimated storage term. This is equivalent to the sum of the turbulent fluxes, and the value should range between 0 and 1. Again the LUMPS estimate shows better agreement with the observations, suggesting these measurements fit well with other urban observations.

In examining the data over the entire field campaign (DOY 229–246) it is seen that the patterns in flux partitioning are essentially the same even though there are greater differences in the times and synoptic conditions over which the fluxes were measured (Table 5). Sensible heat flux at CBD is more than one-half of net radiation, decreasing to slightly less than one-half at IND and less than 35% at the other two sites. Latent heat fluxes show the opposite trend for the sites. For daytime conditions only, the patterns also remain unchanged although the Bowen ratio increases. The midday Bowen ratio, which is expected to be the highest, is still below the LUMPS prediction given in Fig. 6 for the CBD site but matches closely for the other sites.

These results agree with what has been found in other urban campaigns in terms of relations to surface cover. Schmid et al. (1991) attributed differences in  $Q_H/Q^*$  between sites in a residential area as being a result of the amount of vegetation in the source area. They also noted that this and the other flux ratios examined here are not constant in time but exhibit a large degree of variability that may be attributed to the size and makeup of the source area for one particular measurement, as is shown in Figs. 6 and 7.

Estimation of the storage heat flux is difficult in urban areas because of the complexity of the surface at the microscale (e.g., materials, orientations), and we are not able to directly measure it at the local scale. If energy balance closure is assumed then the residual can be used to determine  $\Delta Q_S$ . This accumulates all of the errors and the unmeasured terms of the SEB into the residual  $\Delta Q_S$  (Grimmond and Oke 1999b). An estimate of  $\Delta Q_S$  for CBD, independent of the turbulent flux measurements (Offerle et al. 2005b), ranged from  $-6$  to  $5 \text{ W m}^{-2}$  for any 5-day period during the campaign. The most positive value coincided with the dry period. Although actual  $\Delta Q_S$  will differ between the sites, here all sites have a positive residual, that is,  $\Delta Q_S = Q^* + Q_F - (Q_H + Q_E) > 0$ , over the period of the field campaign (Table 5) even if the anthropogenic heat flux  $Q_F$  is assumed to be zero. A lack of closure is a common occurrence in eddy covariance measurements of the surface energy balance (Wilson et al. 2002). Based on analysis of  $\Delta Q_S$  and  $Q_F$  at the CBD for different times of year it does not appear to be a large problem, but there may be some underestimation of peak turbulent fluxes when  $Q_F$  and  $\Delta Q_S$  are taken into account (Offerle et al. 2005b). The ratio of the residual  $\Delta Q_S$  to  $Q^*$

for the sites ranges from 0.05 (CBD) to 0.16 (IND) (Table 5). The daytime differences suggest that more heat is stored and released on a diurnal basis at the more built areas (IND and CBD), with RUR having low releases. However, the RES site has a value as large as that of the CBD site. Assuming that the mean residual at each site is due to daytime underestimation of turbulent fluxes, in terms of daytime  $\Delta Q_s/Q^*$  the sites are ordered more nearly as expected from the most built up (IND and CBD) to the least (RUR).

#### 4. Conclusions

The objective of this study was to consider the relation of surface characteristics within a city to turbulent heat flux partitioning. Data were collected under summertime conditions in areas that range from 100% grass (RUR) to three urban land use/land cover classes (RES, IND, CBD) within the city of Łódź. These data can provide insight not only about the spatial variability of energy partitioning that can be expected across a city but also about how that variability compares to that documented between cities.

The empirical results showed that temperature differences between the sites were small except when compared with a rural reference. This difference was comparable to previously observed urban–rural differences and is attributable to local surface characteristics. Smaller differences well above the surface are seen as larger-scale effects of urban characteristics on the boundary layer. Diurnal differences in net radiation between the sites were also small except in comparison with the rural site.

Flux partitioning in relation to surface characteristics is in agreement with that observed from other studies both within and among cities. Bowen ratios averaged for the sites show an inverse relation with increasing vegetation, as expected, and latent heat fluxes at the residential site were less dependent on short-term rainfall than at the grass site. The relation between the Bowen ratio and vegetation resulted in values that were very similar to those that have been found between cities (Grimmond and Oke 2002) and within a city (Christen and Vogt 2004). At low fractions of vegetation cover, these values have Bowen ratios that are lower than a potential Bowen ratio. This result implies that when the urban vegetation is sparse or patchy, it transpires at a higher relative rate than does a completely vegetated surface. This situation is readily understood from a microclimatic viewpoint (Oke 1988). Such subgrid-scale effects may require physical parameters for urban vegetation to be altered in numerical models applied to urban surfaces. For example, using a

tile scheme the evaporation rates for the vegetated fractions may be underpredicted when the areal fraction is less than 30% of the grid.

One should expect these patterns to remain similar across cities, although type and moisture status of vegetation must be considered. A nontranspiring or senescent vegetated surface should not behave much differently than a rough impervious surface. This fact explains the power of simple models using modified combination formulations (e.g., Grimmond and Oke 2002) to explain flux partitioning in urban areas over a wide range of sites and vegetation coverage.

Sensible heat fluxes had a positive relation with impervious surface cover and followed the results of previous studies as well. The relation between point-flux measurements and estimated source-area characteristics was weaker but still apparent despite the uncertainty in the source-area estimation. The role of heat storage is clearly important and varies between the sites in relation to the surface characteristics.

These results have important implications for meso-scale modeling. Because computational grid resolution can now easily identify “urban” from “rural,” it is now important to resolve the differences within a city. This study’s data are to be used to evaluate land surface and remote sensing models that can provide the SEB partitioning and mesoscale forcing across whole cities. To date, models such as Masson’s (2000) Town Energy Balance model have tended to be assessed at a point rather than at multiple sites across a city. It is critical that land surface schemes can reproduce the spatial differences identified here that occur under conditions of similar atmospheric forcing. This study also helps to move toward resolving the issue of the number of urban classes that are needed in surface databases. As noted here, these locations can be described in a number of different ways (Table 2); some of the current classifications do allow for spatial distinction within a city. It is clear, however, that the surface databases that are available for urban areas are still in need of much attention to ensure we can use them for urban climate modeling and description both between and within cities.

*Acknowledgments.* Funding for this research was provided by the Polish Academy of Science, NSF 0095284, NSF 0221105, and NATO 977460. NASA provided for the acquisition of ASTER imagery during the field campaign. Professor Catherine Souch provided instrumentation to support this project. We thank the following for providing access to the measurement locations: “Lotnisko Łódź Lublinek,” Ltd., Jednostka Ratowniczo-Gaśnicza nr 10 Państwowej Straży Pożarnej w

Łódź, and Polska Telefonia Komórkowa Centertel, Ltd.

#### REFERENCES

- Abrams, M., S. Hook, and B. Ramachandran, 2002: ASTER user handbook version 2. NASA JPL, 135 pp. [Available online at <http://asterweb.jpl.nasa.gov/>.]
- Auer, A. H., 1978: Correlation of land use and cover with meteorological anomalies. *J. Appl. Meteor.*, **17**, 636–643.
- Best, M. J., 2005: Representing urban areas within operational numerical weather prediction models. *Bound.-Layer Meteor.*, **114**, 91–109.
- Broetzge, J. A., and C. E. Duchon, 2000: A field comparison among a domeless net radiometer, two four-component net radiometers, and a domed net radiometer. *J. Atmos. Oceanic Technol.*, **17**, 1569–1582.
- Christen, A., and R. Vogt, 2004: Energy and radiation balance of a central European city. *Int. J. Climatol.*, **24**, 1394–1421.
- de Bruin, H. A. R., and A. A. M. Holtslag, 1982: A simple parameterization of surface fluxes of sensible and latent heat during daytime compared with the Penman–Monteith concept. *J. Appl. Meteor.*, **21**, 1610–1621.
- Ellefsen, R., 1990: Mapping and measuring buildings in the canopy boundary layer in ten U.S. cities. *Energy Build.*, **15–16**, 1025–1049.
- Grimmond, C. S. B., and C. Souch, 1994: Surface description for urban climate studies: A GIS based methodology. *Geocarto Int.*, **1**, 47–59.
- , and T. R. Oke, 1999a: Aerodynamic properties of urban areas derived from analysis of surface form. *J. Appl. Meteor.*, **38**, 1262–1292.
- , and —, 1999b: Heat storage in urban areas: Observations and evaluation of a simple model. *J. Appl. Meteor.*, **38**, 922–940.
- , and —, 2002: Turbulent heat fluxes in urban areas: Observations and a local-scale urban meteorological parameterization scheme (LUMPS). *J. Appl. Meteor.*, **41**, 792–810.
- , S. K. Potter, H. N. Zutter, and C. Souch, 2001: Rapid methods to estimate sky view factors applied to urban areas. *Int. J. Climatol.*, **21**, 903–913.
- , J. A. Salmond, T. R. Oke, B. Offerle, and A. Lemonsu, 2004: Flux and turbulence measurements at a dense urban site in Marseille: Heat, mass (water, carbon dioxide), and momentum. *J. Geophys. Res.*, **109**, D24101, doi:10.1029/2004JD004936.
- Kaimal, J. C., and J. J. Finnigan, 1994: *Atmospheric Boundary Layer Flows*. Oxford University Press, 289 pp.
- Kaminsky, K. Z., and R. Dubayah, 1997: Estimation of surface net radiation in the boreal forest and northern prairie from short-wave flux measurements. *J. Geophys. Res.*, **102**, 29 707–29 716.
- Klysik, K., 1996: Spatial and seasonal distribution of anthropogenic heat emissions in Łódź, Poland. *Atmos. Environ.*, **30**, 3397–3404.
- , and K. Fortuniak, 1999: Temporal and spatial characteristics of the urban heat island of Łódź, Poland. *Atmos. Environ.*, **33**, 3885–3895.
- Lemonsu, A., C. S. B. Grimmond, and V. Masson, 2004: Modeling the surface energy balance of an old Mediterranean city core. *J. Appl. Meteor.*, **43**, 312–327.
- Liang, S., 2000: Narrowband to broadband conversions of land surface albedo: I. Algorithms. *Remote Sens. Environ.*, **76**, 213–238.
- Martilli, A., A. Clappier, and M. W. Rotach, 2002: An urban surface exchange parameterisation for mesoscale models. *Bound.-Layer Meteor.*, **104**, 261–304.
- Masson, V., 2000: A physically-based scheme for the urban energy balance in atmospheric models. *Bound.-Layer Meteor.*, **94**, 357–397.
- , C. S. B. Grimmond, and T. R. Oke, 2002: Evaluation of the Town Energy Balance (TEB) scheme with direct measurements from dry districts in two cities. *J. Appl. Meteor.*, **41**, 1011–1026.
- Offerle, B., C. S. B. Grimmond, K. Fortuniak, T. R. Oke, and K. Klysik, 2005a: Temporal variability in heat fluxes over a central European downtown. *Theor. Appl. Climatol.*, doi:10.1007/s00704-005-0140-5.
- , —, and —, 2005b: Heat storage and anthropogenic heat flux in relation to the energy balance of a central European city center. *Int. J. Climatol.*, **25**, 1405–1419.
- Oke, T. R., 1987: *Boundary Layer Climates*. Routledge, 435 pp.
- , 1988: The urban energy balance. *Prog. Phys. Geogr.*, **12**, 471–508.
- Panofsky, H. A., and J. A. Dutton, 1984: *Atmospheric Turbulence*. John Wiley and Sons, 397 pp.
- Priestley, C. H. B., and R. J. Taylor, 1972: On the assessment of surface heat flux and evaporation using large-scale parameters. *Mon. Wea. Rev.*, **100**, 81–92.
- Raupach, M. R., 1994: Simplified expressions for vegetation roughness length and zero-plane displacement as functions of canopy height and area index. *Bound.-Layer Meteor.*, **71**, 211–216.
- Ross, S. L., and T. R. Oke, 1988: Tests of 3 urban energy-balance models. *Bound.-Layer Meteor.*, **44**, 73–96.
- Schmid, H. P., 1994: Source areas for scalars and scalar fluxes. *Bound.-Layer Meteor.*, **67**, 293–318.
- , and C. R. Lloyd, 1999: Location bias of flux measurements over inhomogeneous areas. *Agric. For. Meteorol.*, **93**, 195–209.
- , H. A. Cleugh, C. S. B. Grimmond, and T. R. Oke, 1991: Spatial variability of energy fluxes in suburban terrain. *Bound.-Layer Meteor.*, **54**, 249–276.
- Schotanus, P., F. T. M. Nieuwstadt, and H. A. R. DeBruin, 1983: Temperature measurement with a sonic anemometer and its application to heat and moisture fluctuations. *Bound.-Layer Meteor.*, **26**, 81–93.
- Theurer, W., 1999: Typical building arrangements for urban air pollution modelling. *Atmos. Environ.*, **33**, 4057–4066.
- Thorsson, S., and I. Eliasson, 2003: An intra-urban thermal breeze in Göteborg, Sweden. *Theor. Appl. Climatol.*, **75**, 93–104.
- van Dijk, A., W. Kohsiek, and H. A. R. de Bruin, 2003: Oxygen sensitivity of krypton and Lyman- $\alpha$  hygrometers. *J. Atmos. Oceanic Technol.*, **20**, 143–151.
- Webb, E. K., G. I. Pearman, and R. Leuning, 1980: Correction of flux measurements for density effects due to heat and water vapour transfer. *Quart. J. Roy. Meteor. Soc.*, **106**, 85–100.
- Wilson, K., and Coauthors, 2002: Energy balance closure at FLUXNET sites. *Agric. For. Meteorol.*, **113**, 223–243.